Journal of Biomedical Optics

SPIEDigitalLibrary.org/jbo

Design of refractive index sensors based on the wavelength-selective resonant coupling phenomenon in dual-core photonic crystal fibers

Bing Sun
Ming-Yang Chen
Yong-Kang Zhang
Ji-chang Yang

SPIE

Design of refractive index sensors based on the wavelength-selective resonant coupling phenomenon in dual-core photonic crystal fibers

Bing Sun, Ming-Yang Chen, Yong-Kang Zhang, and Ji-chang Yang
Jiangsu University, School of Mechanical Engineering, Department of Optical Engineering, Zhenjiang 212013, Jiangsu Province, China

Abstract. Design strategies for high-sensitivity refractive index sensors based on the principle of wavelength-selective resonant coupling in dual-core photonic crystal fibers are presented. Phase matching at a single wavelength can be achieved between an analyte-filled microstructured core and a small core with a down-doped rod or one small air hole in the center, thus enabling selectively directional resonant-coupling between the two cores. The transmission spectra of the output light presents a notch at the index-matched wavelength, yielding a resonant wavelength depending on the refractive index of the analyte. Numerical simulations demonstrate that both of the two proposed sensors can be used for highly sensitive detection of low-index analyte. In particular, the configuration realized by introducing the fiber with a small air hole in one core can be used to the detection of the analyte index around 1.33 and the sensitivity reach to 1.2×10^4 nm per refractive index unit (RIU). In addition, the detection limit is as low as 2.5×10^{-7} RIU at $n_a = 1.33$. [DOI: 10.1117/1.JBO.17.3.037002]

Keywords: dual core photonic crystal fiber; resonant coupling; notch; refractive index sensor.

Paper 11434 received Aug. 10, 2011; revised manuscript received Jan. 12, 2012; accepted for publication Jan. 13, 2012; published online Mar. 13, 2012.

1 Introduction

Optical fiber sensors are widely employed in chemical and biological applications.[1–4] In recent years, photonic crystal fibers (PCFs) with unique light guiding properties, unprecedented degrees of freedom in tailoring their modal and coupling properties, have been successfully applied to the sensing fields. As their holes can be controllably filled with ultrasmall volumes of analytes, PCFs enable high interaction between the resonant mode and the analyte.[5–8] In particular, PCF refractive index sensors have been explored. For example, Phan Huy et al. have shown that a fiber-sensing system based on photowriting fiber Bragg gratings in a six-hole PCF can achieve a detection limit of 4×10^{-3} RIU for analyte refractive index close to 1.33.[9] In 2008, Rindorf and Bang[10] have applied a photonic crystal fiber long-period grating for the detection of the refractive index of Methanol, thus achieving high sensitivity for chemical sensing.

Since Mangan et al.[11] fabricated a dual-core photonic crystal fibers (DC-PCFs) for the first time, the use of DC-PCFs for realizing fiber couplers have been investigated experimentally[12] as well as theoretically.[13–17] The operation of PCF coupler typically involves energy transfer over a certain coupling length between the two fiber cores coupled by proximate interactions. Furthermore, due to the flexibility of design and ease of fabrication, DC-PCFs are advantageous for applications in highly sensitive sensing. In particular, sensors based on DC-PCF configurations have been shown to be capable of achieving enhanced sensitivity for refractive index sensing.[18–25] Wu et al.[21] demonstrated a high-index DC-PCF sensor, which is based on measuring the shift of the resonant wavelength between the higher-order mode and the fundamental mode. A detection limit of 4.6×10^{-7} RIU with a sensitivity of 30,100 nm/RIU has been demonstrated. However, the device is restricted to measuring analyte index higher than the silica host. Later, it has been shown that coating the holes and using flourinated polymer microstructured optical fibers can extend the detection regime to low-index analytes, such as water.[22] Recently, a dual-core microstructured optical fiber realized by using the exponential dependence of intercore coupling on analyte refractive index, shows the potential for use over a wide range of analyte refractive index with high sensitivity.[23] In the cases of biological and medical applications, analytes are water based solutions, with refractive index in the range of 1.33 to 1.35. As a consequence, the evanescent field propagating through such low-index analytes cannot be well confined and enhanced, which results in the difficulty in designing low-index sensors. Recently, we proposed a DC-PCF with an analyte-filled microstructure.[25] The fiber can detect analyte with a refractive index as low as 1.33. A detection limit of 2.02×10^{-6} RIU and a sensitivity of 8500 nm/RIU can be realized. Sensing in the configuration is based on the index-matched coupling between a solid core and an anlyte-filled microstructured core. However, the diameters of airholes in the microstructured core are only 1 μm, which will increase the difficulty in filling analytes effectively. The increase of airhole diameters in that configuration will lead to lower effective index of the modes in microstructured core, therefore, index-matched coupling cannot be realized. To accomplish that, we proposed an improved optical fiber sensor configuration, the solid core of which is replaced by a small airhole or low-index rod. The introduction of a small airhole or a down-doped rod in one core of the fiber enables more freedom

Address all correspondence to: Ming-Yang Chen, Jiangsu University, School of Mechanical Engineering, Department of Optical Engineering, Zhenjiang 212013, Jiangsu Province, China. Tel: (86)13812457092; E-mail: miniyoung@163.com

0091-3286/2012/$25.00 © 2012 SPIE

in tuning the configuration and the large airholes in the other core can also lead to more effective filling of the analyte. In addition, the difference between the features of the two sensors is investigated, and the tolerance of the fiber length for the two fibers is also presented.

2 Numerical Simulation

To obtain highly sensitive index sensing, the overlap between the resonant mode and the analyte should be enhanced. Overlap is most simply understood as the fraction of optical power that is exposed to the analyte. It should be noted that the liquid core index-guided fiber can increase the optical power to overlap with the analyte.[7] However, the fraction of optical power will extend to the background of the fiber when only a hole in the center of the core is filled with the analyte. As a consequence, it will result in a reduced overlap between the analyte and the fundamental mode of the core.[25] As expected, the introduction of microstructured core can help to increase the amount of energy that travels in the holes where the analyte can be filled.[25,26] This is due to the fact that the optical power will be more evenly distributed in the analyte-filled microstructure than that of an analyte-filled hole, as a result, it will improve the overlap with the analyte and thus sensitivity. Figure 1 shows the cross-section of a dual-core photonic crystal fiber. The diameters of the cladding holes and the analyte-filled holes are set as d. The refractive index of the analyte is set as n_a. Supposing that the phase-matching between the two modes of the conventional PCF core (small core) and the analyte-filled microstructured core (large core) is reached, maximum power transfer over a coupling length occurs at the index-matched wavelength, namely, the resonant wavelength. As a result, the spectral transmission of the small core presents a notch corresponding to the resonant wavelength, when a broadband beam is launched into the small core. It should be noted that the notch is dependent on the analyte's index.

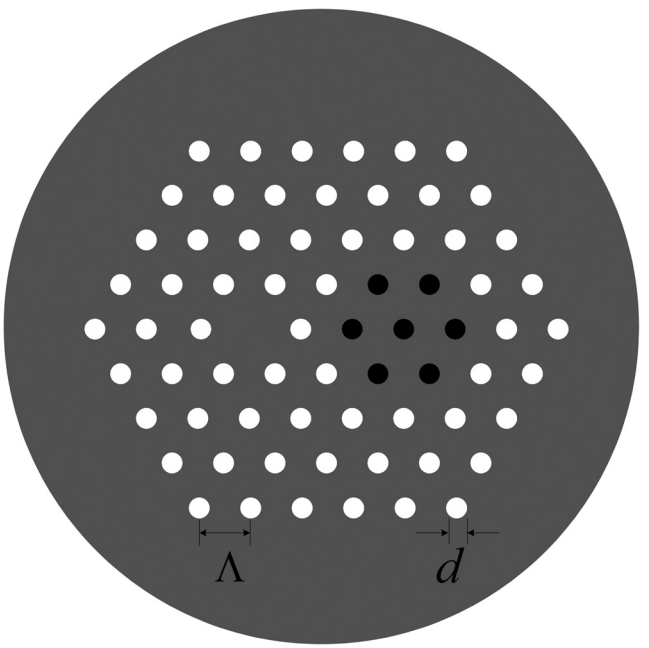

Fig. 1 Cross-section of a dual-core photonic crystal fiber. The gray area denotes pure silica, the white area represents air holes and the dark region respresents the analyte.

Figure 2 plots the effective indices of the fundamental modes in the two cores of the dual-core PCF shown in Fig. 1. As shown in Fig. 2, the phase matching cannot be realized in the normalized frequency range owing to the obviously large mode indices difference and the index difference between the two cores is always very large. The index difference decreases with the increase of normalized frequency. Therefore, it is only possible to achieve index match at very high frequency. In this way, the fiber coupling length should be increased and then result in long filling length, which will increase the filling time and volumes of analytes needed.

However, the previously mentioned problem can be solved by two methods: to introduce a down-doped rod into the small core, or to introduce a small airhole into the small core. Both methods can reduce the effective index of the fundamental mode in the small core, so index-matched coupling can be reached. In this section, we will apply the first method and define the corresponding structure as Fiber I, the cross-section of which is depicted in Fig. 3. Core A is composed of a down-doped rod embedded in the background of silica. The refractive index of the background material and the down-doped rod index are set as n_c and n_r. The diameter of the rod is set as w and the doping level of the down-doped rod is defined as $\Delta_d = n_r - n_c$. Core B is a microstructured core, which is composed of seven analyte-filled holes embedded in a silica background. The refractive index of the analyte is set as n_a. The center-to-center distance of the two nearest airholes is set as Λ. We define the diameters of the cladding holes and the analyte-filled holes as d and set it as $d = 0.5\Lambda$.

We solve the modes of the individual cores in the proposed Fiber I by semivectorial beam propagation method (BPM).[27] Figure 4 plots the effective indices of the fundamental modes in the two cores of the dual-core PCF with $w/\Lambda = 0.9$ and $\Delta_d = -0.007$. Owing to the fact that phase matching is reached at the normalized frequency where $\Lambda/\lambda = 4.185$, we expect the effective coupling can appear at this point. Therefore, if the resonant coupling happens at the wavelength of 1550 nm, the corresponding pitch Λ should be 6.487 μm. Therefore, the diameters of the analyte-filled airholes should be 3.24 μm. The airhole diameter of our previously reported DC-PCF sensor is only

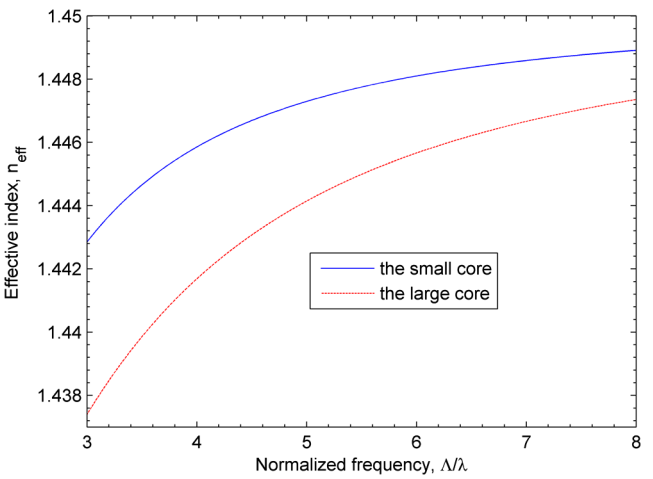

Fig. 2 The fundamental effective index curves of the small core (solid curve) and large core (dashed curve) for the vertical polarization with $d/\Lambda = 0.5$, and $n_a = 1.33$.

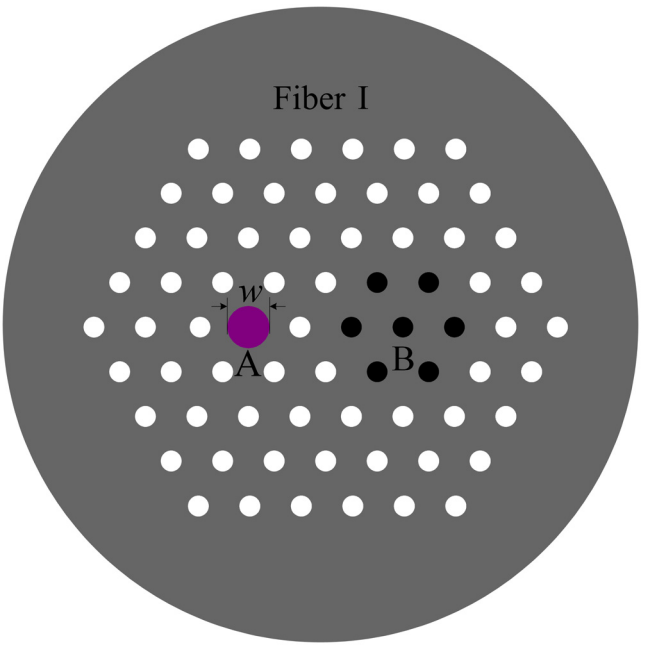

Fig. 3 The cross-section of the proposed Fiber I.

1 μm. The proposed configuration can effectively reduce the difficulty of filling the analyte in small airhole PCF.

Here we will consider only the coupling characteristics of the vertically polarized state. The horizontally polarized mode can be eliminated by inserting a polarizer before the optical spectrum analyzer (OSA).[21] The coupling length of the structure at the wavelength of 1550 nm is $L_c = 22.24$ mm. We calculate the transmission characteristic of Fiber I with fiber length $L = 22.24$ mm through the semivectorial BPM. Figure 5 shows the evolution of the normalized power transmission at core A as a function of the operating wavelength for $n_a = 1.33$ when the vertically polarized fundamental mode is launched into the core A. The transmission spectra of the coupler presents a notch at the resonant wavelength where the two fundamental modes of the fiber are phase-matched. The sensitivity of the resonant-based sensor is defined as $S = \partial\lambda_r/\partial n_a$ and the detection limit is formulated as $\delta n_L \approx 3/4.5 \times \lambda_{\mathrm{FWHM}}/(S \times \mathrm{SNR}^{0.25})$,

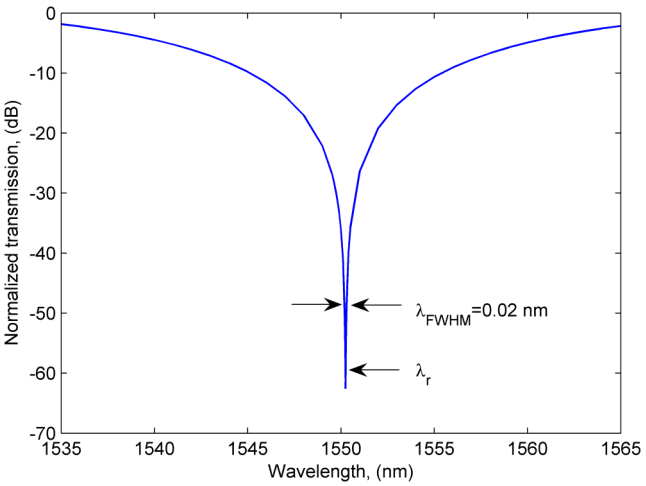

Fig. 5 Normalized transmission spectra of core A for Fiber I.

where λ_{FWHM} is the full-width half-max of the mode amplitude, SNR is in linear units [e.g., 50 dB gives $10^{(50/10)}$].[28] The shift of the transmission resonance notch between $n_a = 1.33$ and $n_a = 1.331$ is 6.54 nm, which corresponds to a sensitivity of $S = 6.54 \times 10^3$ nm/RIU. The spectral width λ_{FWHM} of the resonance notch at $n_a = 1.33$ is only 0.02 nm. Assuming a signal-to-noise ratio of 50 dB, we can get a detection limit of 1.15×10^{-7} RIU.

It is true that the sensitivity of Fiber I is not high, which is explained based on the slope of the mode index curves of the two cores. As can be seen from Fig. 4, the slope of mode index curve of core A is smaller than that of core B and there is a large difference between the slopes of the two curves. Therefore, increasing or decreasing the index of analyte cannot lead to large shift in resonant wavelength. Obviously, a smaller difference between the slopes of the two curves can effectively increase the shift of the resonant wavelength. For this purpose, we adopt another structure where the down-doped rod in Fiber I is replaced by a small airhole and define it as Fiber II. Fiber II is constructed by using the same configuration as Fiber I except that the diameter of the small airhole in Fiber II is set as d_c. Figure 6 shows the mode index curves between the two

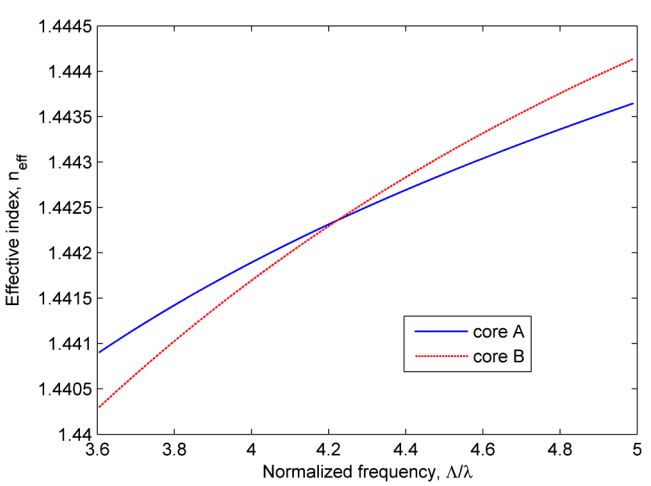

Fig. 4 Effective indexes curves of core A and core B for the vertical polarization in Fiber I with $w/\Lambda = 0.9$ and $\Delta_d = -0.007$.

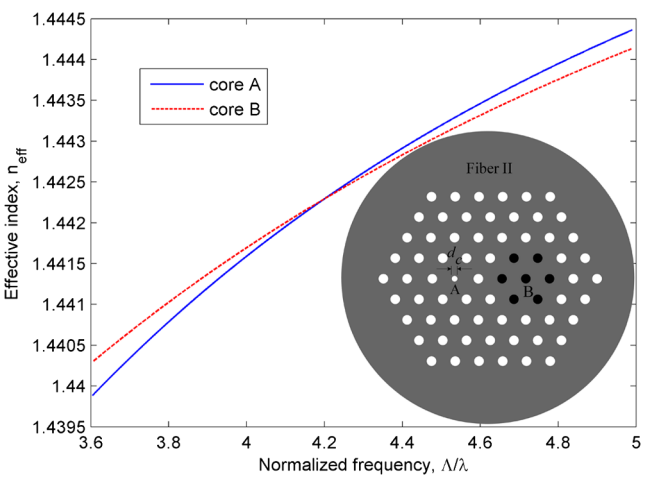

Fig. 6 Effective indexes curves of core A and core B for the vertical polarization of Fiber II with $d/\Lambda = 0.5$, $d_c/\Lambda = 0.3$, and $n_a = 1.33$. The inset shows the cross-section of Fiber II.

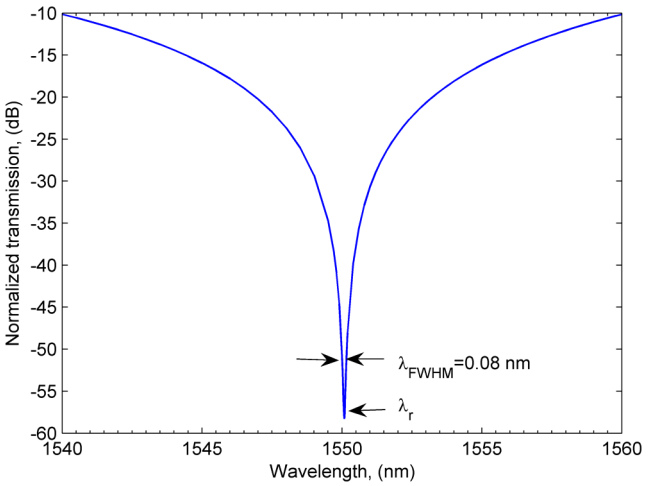

Fig. 7 Normalized transmission spectra of core A for Fiber II.

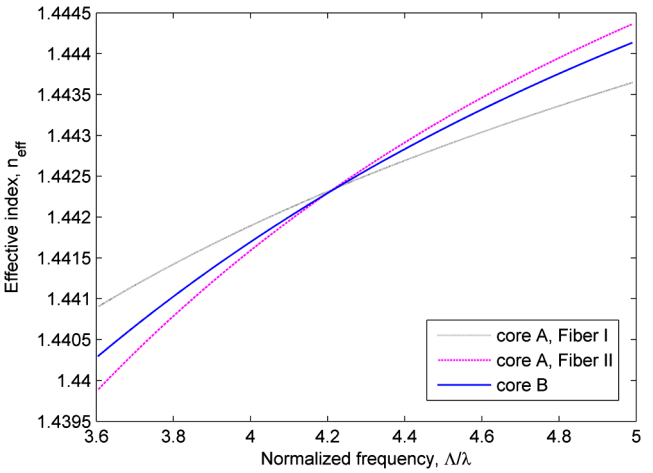

Fig. 9 The effective index curves of the fundamental modes for Fiber I and Fiber II.

cores in Fiber II, the inset shows the cross-section of Fiber II. To compare these two structures, we also set the period of Fiber II to be $\Lambda = 6.487\ \mu$m and the index of analyte as $n_a = 1.33$. By requiring that the index-matched coupling will also be met at the wavelength of 1550 nm for Fiber II, we get the diameter of the small airhole to be $d_c/\Lambda = 0.3$. The calculated coupling length of Fiber II at the wavelength of 1550 nm is 20.33 mm.

Figure 7 shows the spectral transmission of core A in Fiber II while the fiber length is set as 20.33 mm. The shift of the resonant wavelength, λ_r, between 1.330 and 1.331 is 12 nm, which corresponds to a sensitivity of $S = 1.2 \times 10^4$ nm/RIU. Simulation at $n_a = 1.330$ gives a resonant feature of spectral width $\lambda_{\mathrm{FWHM}} = 0.08$ nm. Assuming a signal-to-noise ratio of 50 dB, we get a detection limit of 2.5×10^{-7} RIU. It's obvious that the sensitivity of Fiber II is better than Fiber I, although the detection limit gets a little worse.

3 Discussion

3.1 *Sensitivities and Detection Limits of Fiber I and Fiber II for Different Analytes*

The aforementioned analysis of sensitivities and detection limits for Fiber I and Fiber II are limited to the analyte with $n_a = 1.33$. In fact, the potential for refractive index sensing over a wide dynamic range is an important indicator for a refractive index sensor. The detection limits and sensitivities as a function of analyte index have been investigated when fiber lengths are fixed at 22.24 mm and 20.33 mm for Fiber I and Fiber II, respectively. It can be seen from Fig. 8 that the sensitivity of Fiber I improves with the increased analyte index, whereas the sensitivity of Fiber II is only slightly decreased with the increased analyte index. Furthermore, both the detection limits get worse when the analyte index is away from 1.33. By requiring the detection limit be lower than 2×10^{-5} RIU, we can then get the dynamic range of Fiber I is $\Delta n = 0.017$ ranging from 1.323 to 1.340 and the dynamic range of Fiber II is $\Delta n = 0.01$ ranging from 1.325 to 1.335.

We can see that Fiber I has a wider dynamic range than Fiber II, which can be attributed to the fact that the variation of the resonant coupling length of Fiber I is smaller than that of Fiber II. In further attempts to explain what caused the changes of coupling lengths for Fiber I and Fiber II, we plot in Fig. 9 that the refractive indices of the fundamental mode of core A and core B in Fiber I and Fiber II, respectively, and we can see that the slope of core A is smaller than that of core B for Fiber I, while the slope of core A is larger than that of core

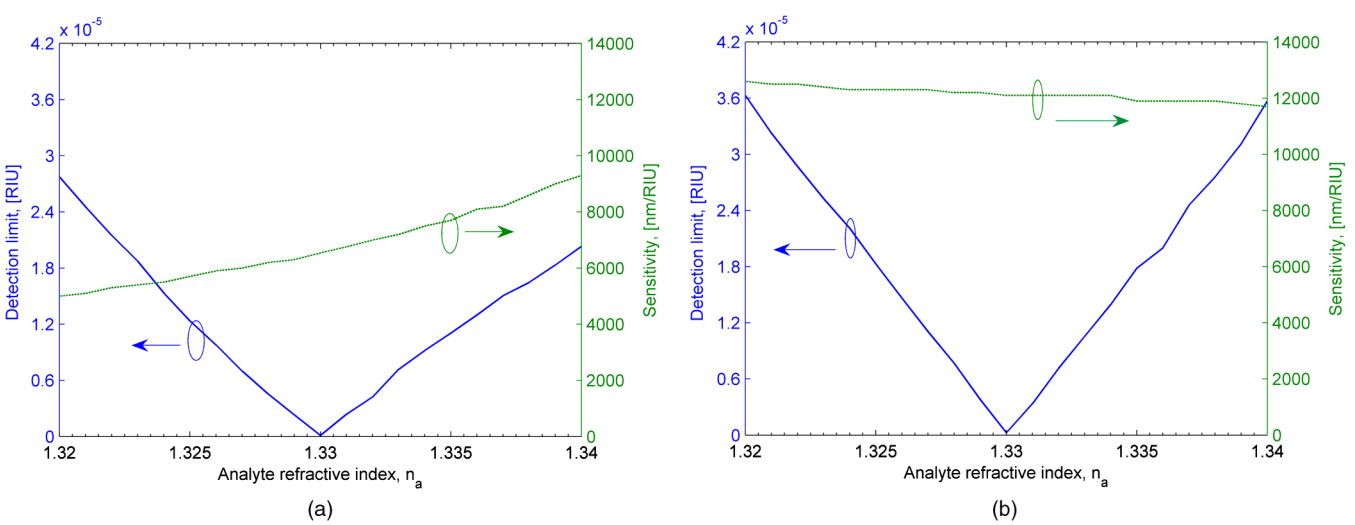

Fig. 8 Variation of detection limits and sensitivities as a function of analyte index for (a) Fiber I and (b) Fiber II.

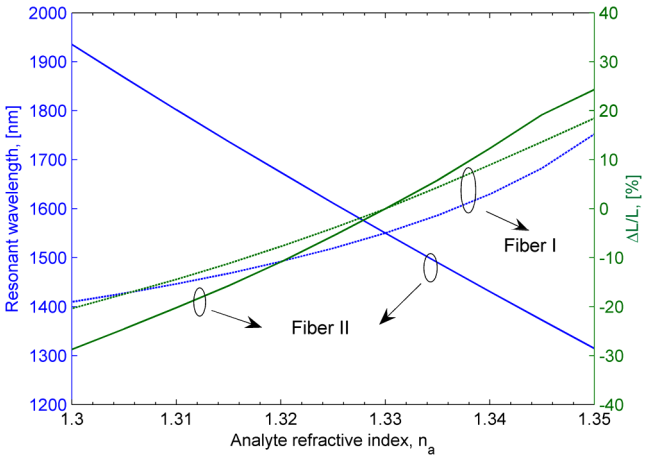

Fig. 10 Resonant wavelength and the change in coupling length as a function of analyte refractive index for Fiber I and Fiber II. The blue lines represent the change in coupling length and the green lines denote resonant wavelengths.

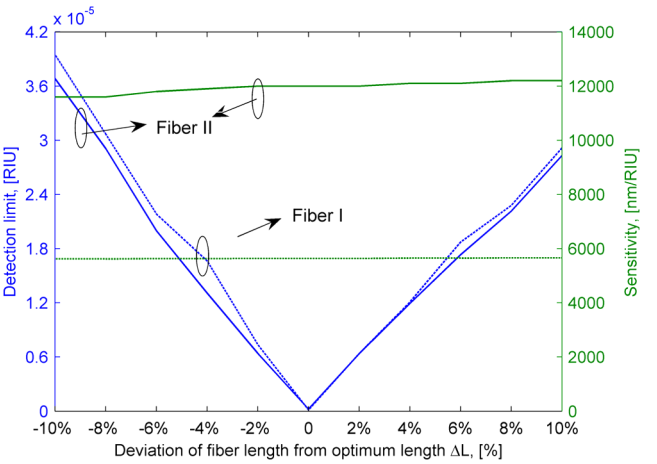

Fig. 11 Variation of sensitivity and detect limit as a function of deviation of fiber length from the optimum length for Fiber I and Fiber II. The blue lines denote detection limit and the green lines represent sensitivity.

B for Fiber II. Therefore, the effective index curve of the fundamental mode in core B shifts up when the refractive index of the analyte increases. Thus, it causes the resonant wavelength to shift to longer wavelength for Fiber I and shorter wavelength for Fiber II. Generally, the coupling length for Fiber I and Fiber II should increase with the increase of the analyte's index due to the fact that the evanescent field prefers to stay in the analyte with higher refractive index and hence leads to a weak overlap between the mode fields of the two cores. However, the resonant wavelength shifts to longer wavelength for Fiber I, the confinement of the cladding is weaker, which can lead to the extension of the mode fields, therefore, the overlap between the mode fields of the two cores increases. As a consequence, the increased trend of coupling length can be partly offset by the decreased trend of coupling length owing to the enhanced overlap caused by the shift of the resonant wavelength to longer wavelength for Fiber I. It can be seen from Fig. 10 that the resonant wavelengths of Fiber I and Fiber II shift inversely with the change of the analyte refractive index. The ratio of the variation in coupling length with the variation of the analyte index is also plotted in Fig. 10. It is obvious that the coupling length of Fiber II is more dependent on the analyte's index than that of Fiber I. That is why Fiber I has wider the dynamic range than Fiber II.

3.2 *Tolerance Analysis of Fiber I and Fiber II*

We will focus our discussion on the fiber length tolerances of Fiber I and Fiber II at $n_a = 1.33$. The coupling lengths of Fiber I and Fiber II are calculated at the wavelength of 1.55 μm as 20.33 mm and 22.24 mm, respectively. Figure 11 shows the sensitivities and detection limits of the two sensors with $\pm 10\%$ variation in fiber length with respect to the optimum value. As can be seen from the figure, the deviation of the fiber length from the optimum value leads to a linear increase of the detection limit while both sensitivities are only slightly changed. We can see that the fiber with $\pm 10\%$ variation in fiber length with respect to the optimum value can still have a detection limit lower than 3.95×10^{-5} RIU. Therefore, the proposed fibers allow a relatively large tolerance of length deviation.

3.3 *Solutions for Different Kinds of Analytes*

We present in this manuscript the design of an optical biosensor that can detect analytes with a refractive index lower than the background index of optical fiber, which is not necessarily a water-based solution. The design of optical fiber sensors for highly sensitive detection of such analytes are still a challenge. Generally, operating at a long wavelength is more preferred. For index-guiding optical fiber sensors, more light can be extended to the low-index analytes, which can increase the sensitivity of the sensors. We can also take advantage of the low transmission losses, commercially available light sources, and standard optical fiber components operating around 1550 nm.

As for a water-based solution, we can shift the operating wavelength to the visible spectrum where the absorption loss of water is low. According to the Maxwell equation, the shifting of operating wavelength to visible wavelength in an optical waveguide can be realized by reducing the size of the configuration. For instance, by reducing the period of the airholes in Fiber II to $\Lambda = 3$ μm, and reducing the diameters of airholes in the sensors with the same scale, the operating wavelength of the Fiber II is shifted to around 700 nm.

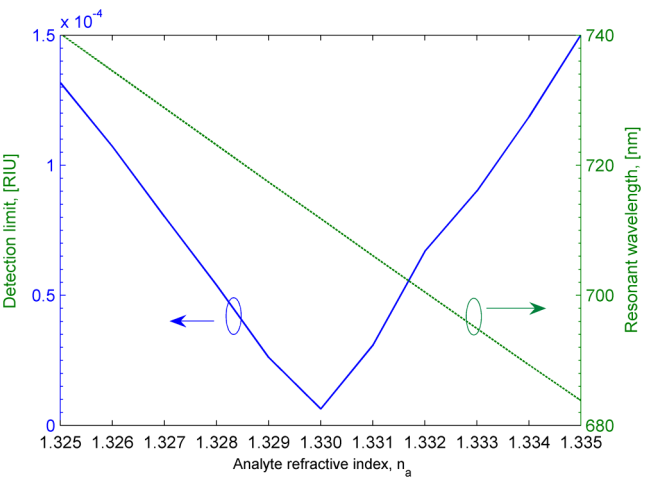

Fig. 12 Variation of sensitivity and detect limit as a function of deviation of analyte refractive index.

The sensitivity and detect limit as a function of deviation of analyte refractive index is shown in Fig. 12. The dynamic range of the sensors is $\Delta n = 0.01$ if the detection limit should be lower than 1.5×10^{-4} RIU. In addition, the sensitivities of the sensor range from 5500 nm/RIU to 5800 nm/RIU for the analyte index in the range of 1.325 to 1.335. Obviously, the sensitivity and detection limit get worse with the blueshift of the operational wavelength. In addition, we can increase the period of the airholes by adjusting the index-matched point. As Fig. 9 shows, the index-matched frequency can be shifted to higher frequency by simply increasing the effective modal index of core A for Fiber I, or decreasing the effective modal index of core A for Fiber II. This technique can remedy the reduction of airhole sizes by working at visible wavelengths.

The refractive index change of the water owing to the variation of temperature during the process of detection is a commonly faced problem for the detection of water-based solution. This problem can be overcome by placing the fiber sensor in a temperature control box.

3.4 *Fluid Selective-Filling*

Fiber sensor designed in this article should be realized by selectively filling holes, while leaving the other airholes unfilled. In fact, there have been some demonstrated techniques to realize selective filling, including collapsing airholes, injection-cleave techniques exploiting the differential filling speeds of holes of different sizes,[29,30] and direct manual gluing.[21,31,32] In particular, the direct gluing technique allows the creation of any arbitrary pattern of filled and unfilled holes. The designed configuration we proposed requires filling fluid into the airholes in core B with all the other airholes unfilled.

4 Conclusion

In conclusion, we proposed two novel PCF configurations designed for refractive index sensors. By filling a microstructured core with the analyte and introducing a down-doped rod or a small airhole into the other core, the fundamental mode indices between the two cores can be matched. By measuring the shift of the index-matched wavelength, the detection of refractive index of the analyte can be achieved. It has been revealed that these two different phase-matching designs lead to large difference between sensitivities of the two fibers. Finally, it has been shown that the two proposed sensors can work with a relatively large fiber length tolerance.

Acknowledgments

This work is supported by the National Natural Science Foundation of China (NNSFC) (Grant No. 10904051); the Qing Lan Project of Jiangsu Province, the China Postdoctoral Science Foundation (Grant Nos. 20080441070 and 200902505); and the Innovation Program of Graduated Student of Jiangsu Province (Grant No. CXZZ11_D547).

References

1. B. Lee, "Review of the present status of optical fiber sensors," *Opt. Fiber Technol.* **9**(2), 57–79 (2003).
2. O. S. Wolfbeis, "Fiber-optic chemical sensors and biosensors," *Anal. Chem.* **76**(12), 3269–3284 (2004).
3. K. L. Brogan and D. R. Walt, "Optical fiber-based sensors: application to chemical biology," *Curr. Opin. Chem. Biol.* **9**(5), 494–500 (2005).
4. G. Gauglitz, "Direct optical sensors: principles and selected applications," *Anal. Bioanal. Chem.* **381**(1), 141–155 (2005).
5. T. M. Monro, D. Richardson, and P. Bennett, "Developing holey fibres for evanescent field devices," *Electron. Lett.* **35**(14), 1188–1189 (1999).
6. T. M. Monro et al., "Sensing with microstructured optical fibres," *Meas. Sci. Technol.* **12**, 854–858 (20010`).
7. J. M. Fini, "Microstructure fibres for optical sensing in gases and liquids," *Meas. Sci. Technol.* **15**(6), 1120–1128 (2004).
8. T. Ritari et al., "Gas sensing using air-guiding photonic bandgap fibers," *Opt. Express* **12**(17), 4080–4087 (2004).
9. P. Huy et al., "Tilted fiber Bragg grating photowritten in microstructured optical fiber for improved refractive index measurement," *Opt. Express* **14**(22), 10359 (2006).
10. L. Rindorf and O. Bang, "Highly sensitive refractometer with a photonic-crystal-fiber long-period grating," *Opt. Lett.* **33**(6), 563–565 (2008).
11. B. Mangan et al., "Experimental study of dual-core photonic crystal fibre," *Electron. Lett.* **36**(16), 1358–1359 (2000).
12. W. MacPherson et al., "Two-core photonic crystal fibre for Doppler difference velocimetry," *Opt. Commun.* **223**(4–6), 375–380 (2003).
13. F. Fogli et al., "Full vectorial BPM modeling of index-guiding photonic crystal fibers and couplers," *Opt. Express* **10**(1), 54–59 (2002).
14. K. Saitoh, Y. Sato, and M. Koshiba, "Coupling characteristics of dual-core photonic crystal fiber couplers," *Opt. Express* **11**(24), 3188–3195 (2003).
15. J. L. Lægsgaard, O. Bang, and A. Bjarklev, "Photonic crystal fiber design for broadband directional coupling," *Opt. Lett.* **29**(21), 2473–2475 (2004).
16. J. Lægsgaard, "Directional coupling in twin-core photonic bandgap fibers," *Opt. Lett.* **30**(24), 3281–3283 (2005).
17. S. K. Varshney et al., "The impact of elliptical deformations for optimizing the performance of dual-core fluorine-doped photonic crystal fiber couplers," *Opt. Express* **14**(5), 1982–1995 (2006).
18. X. Sun, "Wavelength-selective coupling of dual-core photonic crystal fiber with a hybrid light-guiding mechanism," *Opt. Lett.* **32**(17), 2484–2486 (2007).
19. K. Saitoh et al., "Tunable photonic crystal fiber couplers with a thermo-responsive liquid crystal resonator," *J. Lightwave Tech.* **26**(6), 663–669 (2008).
20. D. J. J. Hu et al., "Design and analysis of thermally tunable liquid crystal filled hybrid photonic crystal fiber coupler," *Opt. Commun.* **282**(12), 2343–2347 (2009).
21. D. K. C. Wu, B. T. Kuhlmey, and B. J. Eggleton, "Ultrasensitive photonic crystal fiber refractive index sensor," *Opt. Lett.* **34**(3), 322–324 (2009).
22. B. T. Kuhlmey, S. Coen, and S. Mahmoodian, "Coated photonic bandgap fibres for low-index sensing applications: cutoff analysis," *Opt. Express* **17**(18), 16306–16321 (2009).
23. G. E. Town et al., "Microstructured optical fiber refractive index sensor," *Opt. Lett.* **35**(6), 856–858 (2010).
24. W. Yuan, G. E. Town, and O. Bang, "Refractive index sensing in an all-solid twin-core photonic bandgap fiber," *IEEE Sensor. J.* **10**(7), 1192–1199 (2010).
25. B. Sun et al., "Microstructured-core photonic-crystal fiber for ultrasensitive refractive index sensing," *Opt. Express* **19**(5), 4091–4100 (2011).
26. C. Cordeiro et al., "Microstructured-core optical fibre for evanescent sensing applications," *Opt. Express* **14**(26), 13056–13066 (2006).
27. W. Huang and C. Xu, "Simulation of three-dimensional optical waveguides by a full-vector beam propagation method," *IEEE J. Quant. Electron.* **29**(10), 2639–2649 (1993).
28. I. M. White and X. Fan, "On the performance quantification of resonant refractive index sensors," *Opt. Express* **16**(2), 1020–1028 (2008).
29. K. Nielsen et al., "Selective filling of photonic crystal fibres," *J. Opt A-Pure Appl. Opt.* **7**(8), L13–L20 (2005).
30. Y. Huang, Y. Xu, and A. Yariv, "Fabrication of functional microstructured optical fibers through a selective-filling technique," *Appl. Phys. Lett.* **86**(2), (2005).
31. M. A. Schmidt et al., "Waveguiding and plasmon resonance in two-dimensional photonic lattices of gold and silver nanowires," *Phys. Rev. B* **77**(3), (2008).
32. X. Zhang et al., "Selective coating of holes in microstrucured optical fiber and its application to in-fiber absorptive polarizers," *Opt. Express* **15**(24), 16270–16278 (2007).